JOC Article

Mechanistic Analysis of Intramolecular Free Radical Reactions toward Synthesis of 7-Azabicyclo[2.2.1]heptane Derivatives

Elena Soriano* and José Marco-Contelles

Laboratorio de Radicales Libres y Química Computacional (LRL/QC), IQOG (CSIC), C/Juan de la Cierva 3, 28006 Madrid, Spain

esoriano@iqog.csic.es

Received February 2, 2009

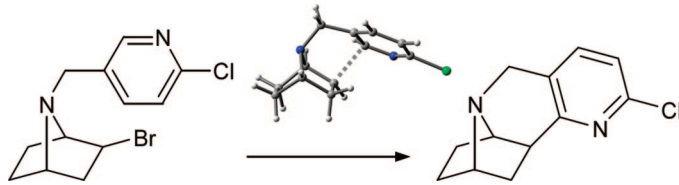

The mechanisms for the formation of conformationally constrained epibatidine analogues by intramolecular free radical processes have been computationally addressed by means of DFT methods. The mechanism and the critical effect of the 7-nitrogen protecting group on the outcome of these radical-mediated cyclizations are discussed. Theoretical findings account for unexpected experimental results and can assist in the selection of proper precursors for a successful cyclization.

Introduction

Epibatidine (Figure 1), an alkaloid isolated from extracts of the skin of the poisonous frog *Epipedobates tricolor*, is a highly potent agonist at several central nervous system nicotinic acetylcholine receptors (nAChRs)[1] and exhibits a potent analgesic activity.[2] Epibatidine has been found to be 200−500 times as potent as morphine, although binding studies with an opioid receptor preparation showed almost 9000 times weaker binding in comparison with [^{3}H]-dihydromorphine.[1]

The intriguing biological activity of epibatidine,[3] bearing an unusual 7-azabicyclo-[2.2.1]heptane skeleton, and the scarcity of epibatidine in nature have stimulated the development of novel, efficient, and stereocontrolled synthetic routes of epibatidine and related analogues, aimed at minimizing toxic effects[4] of epibatidine. Thus, in the past years a number of methodologies have been reported for the total synthesis of epibatidine and 7-azabicyclo[2.2.1]heptane derivatives[5a] and for the synthesis and biological evaluation of epibatidine analogues,[5b] either heterocyclic[6] or conformationally constrained.[7]

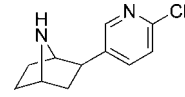

FIGURE 1. Epibatidine.

In this context, we have recently described the synthesis of diversely functionalized 7-substituted *exo*-2-bromo-7-azabicyclo[2.2.1]heptane derivatives, based on a four-step, simple synthetic sequence, starting from readily available cyclohex-3-enecarboxylic acid: Curtius reaction, stereoselective bromination leading to major 7-*tert*-butyl (benzyl) 7-(*cis*-3,*trans*-4-dibromocyclohex-1-yl)carbamates (or 2,2,2-trifluoroacetamides), followed by NaH-mediated intramolecular cyclization (Scheme 1).[8a,b]

This potent and simple methodology has proven very useful for the synthesis of heterocyclic analogues via intermolecular

(1) Holladay, M. W.; Dart, M. J.; Lynch, J. K. *J. Med. Chem.* **1997**, *40*, 4169.
(2) Spande, T. F.; Garraffo, H. M.; Edwards, M. W.; Yeh, H. J. C.; Pannell, L.; Daly, J. W. *J. Am. Chem. Soc.* **1992**, *114*, 3475.
(3) For some selected reviews on the chemistry and biology of epibatidine and epibatidine analogues, see: (a) Daly, J. W. *J. Med. Chem.* **2003**, *46*, 445. (b) Romanelli, M. N.; Gualteri, F. *Med. Res. Rev.* **2003**, *23*, 393. (c) Broka, C. A. *Med. Chem. Res.* **1994**, *4*, 449.
(4) Rao, T. S.; Correa, L. D.; Reid, R. T.; Lloyd, G. K. *Neuropharmacology* **1996**, *35*, 393.
(5) (a) Chen, Z.; Trudell, M. L. *Chem. Rev.* **1996**, *96*, 1179. (b) Carroll, F. I. *Bioorg. Med. Chem. Lett.* **2004**, *14*, 1889.
(6) (a) Seerden, J.-P. G.; Tulp, M. Th. M.; Scheeren, H. W.; Kruse, C. G. *Bioorg. Med. Chem.* **1998**, *6*, 2103. (b) Carroll, F. I.; Robinson, T. P.; Brieaddy, L. E.; Atkinson, R. N.; Mascarella, S. W.; Damaj, M. I.; Martín, B. R.; Navarro, H. A. *J. Med. Chem.* **2007**, *50*, 6383, and references therein.
(7) (a) Brieaddy, L. E.; Mascarella, S. W.; Navarro, H. A.; Atkinson, R. N.; Damaj, M. I.; Martín, B. R.; Carroll, F. I. *Tetrahedron Lett.* **2001**, *42*, 3795. (b) Abe, H.; Arai, Y.; Aoyagi, S.; Kibayashi, C. *Tetrahedron Lett.* **2003**, *44*, 2971. (c) Wei, Z.-L.; Petukhov, P. A.; Xiao, Y.; Tückmantel, W.; George, C.; Kellar, K. J.; Kozikowski, A. P. *J. Med. Chem.* **2003**, *46*, 921.
(8) (a) Gómez-Sánchez, E.; Marco-Contelles, J. *Lett. Org. Chem.* **2006**, *3*, 827. (b) Gómez-Sánchez, E.; Soriano, E.; Marco-Contelles, J. *J. Org. Chem.* **2007**, *72*, 8656. See also the pioneering studies: (c) Bastable, J. W.; Cooper, A. J.; Dunkin, I. R.; Hobson, J. D.; Ridell, W. D. *J. Chem. Soc., Perkin Trans. 1* **1981**, 1339. (d) Kapferer, P.; Vasella, A. *Helv. Chim. Acta* **2004**, *87*, 2764.

10.1021/jo900225f CCC: $40.75 © 2009 American Chemical Society
Published on Web 04/29/2009

SCHEME 1

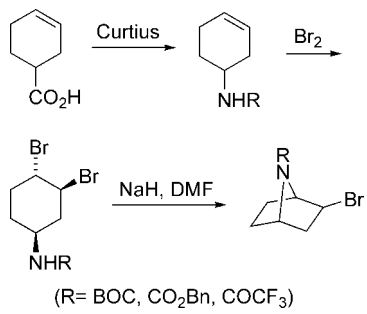

SCHEME 2

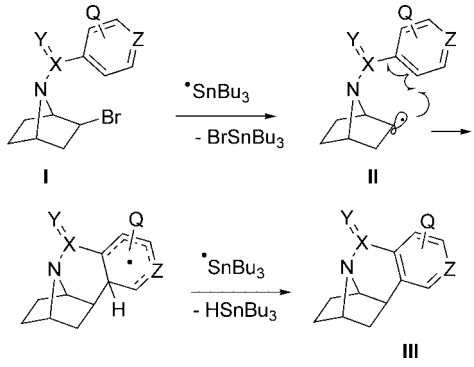

free radical reactions[9] exploiting the rich and unexplored reactivity of 7-azabicyclo[2.2.1]hept-2-yl radicals. Although the synthesis and reactivity of 7-norbornenyl,[10] norborn-5-en-2-yl,[11] and norborn-2-yl[12,13] radicals is well-known, the chemistry of 7-azabicyclo[2.2.1]hept-2-yl radicals has been scarcely investigated. Fraser and Swingle reported the chlorination of 7-trichloroacetyl-7-azabicyclo[2.2.1]heptane with sulfuryl chloride in the presence of benzoyl peroxide.[14]

With this precedent in mind we have designed a simple approach for the synthesis of conformationally constrained epibatidine analogues **III** based on the intramolecular free radical cyclization of species **II** readily available from precursors **I** as they bear suitable radical acceptors at C7 and good leaving groups at C2 (Scheme 2).

Taking into account these precedents, we decided to synthesize and submit to cyclization radical precursors **1**−**5** (Figure 2). Unfortunately, successful results have only been observed for precursors **4** and **5** to give epibatidine analogues **6** and **7** (Figure 2), respectively.[15] When this work was in progress, Armstrong and co-workers reported what appears to be the first intramolecular cyclization of a precursor in this series, namely, *exo*-2-bromo-7-(toluene-4-sulfonyl)-7-azabicyclo[2.2.1]heptane.[16]

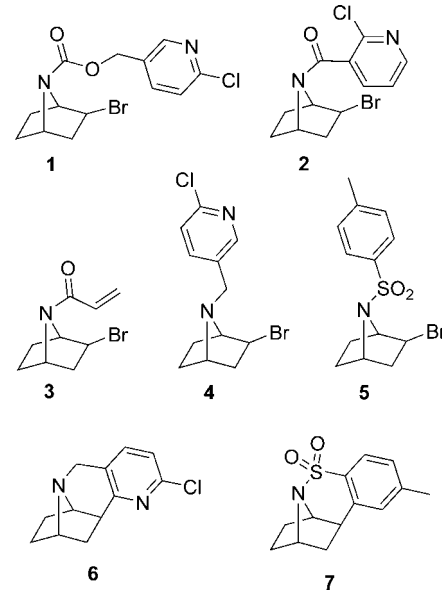

FIGURE 2. Radical precursors and conformationally constrained epibatidine analogues (**6**, **7**).

In this paper, a DFT-based analysis aimed at accounting for these experimental observations is described; in particular, the role of the linker length and flexibility and the aromatic ring. The results should help us in the selection of future precursors for a successful cyclization to the desired target molecules.

Results and Discussion

From the selected precursors (Figure 2), the intramolecular cyclization of carbamate **1** and amides **2** and **3** should be expected a difficult given the low flexibility of the carbamate and amide functionalities due to the effective conjugation. On the other hand, previous results on such molecular skeletons have revealed a moderately low rotational barrier for the -N-CO bond as compared with acyclic amides due to a loss of the resonance stabilization, i.e., the delocalization stabilization of the lone pair electrons of N from the nonbonding n_N orbital to the antibonding $\pi^*_{C=O}$ orbital.[9] This would induce a somewhat higher flexibility in the linker than expected thus allowing the intramolecular cyclization.

However, under the experimental conditions, radical precursor **1**[8a,b] gave the reduced uncyclized product **8** in 36% yield (Scheme 3), but the intramolecular cyclization adduct **9** was not detected. Amide **2** gave the partially reduced, uncyclized derivative **10** and the fully dehalogenated compound **11** (Scheme 3) as the only reaction products.

When precursor **3** was submitted to the free radical conditions, a complex reaction mixture was obtained, and no pure defined compound could be isolated and characterized.

On the basis of these findings, the reactive radical species (denoted by subscript "R") generated under the experimental conditions, $\mathbf{A_R}$, may evolve through two competing reactions (Scheme 4): (a) an intermolecular abstraction of H to form the reduced adducts **B** and (b) an intramolecular cyclization to generate radical $\mathbf{C_R}$, which subsequently would provide, via hydrogen abstraction, the final product (**C**).

For the radical generated from carbamate **1**, namely, $\mathbf{1_R}$, the formation of the reduced species **8** proceeds in an exothermic step (−15.96 kcal mol^{-1}), where the activation barrier to reach the asymmetric transition structure **TS** (C−H = 1.772, Sn−H

(9) Gómez-Sánchez, E.; Soriano, E.; Marco-Contelles, J. *J. Org. Chem.* **2008**, *73*, 6784.
(10) Underwood, G. R.; Friedman, H. S. *J. Am. Chem. Soc.* **1977**, *99*, 27.
(11) (a) Giese, B.; Jay, K. *Chem. Ber.* **1979**, *112*, 298. (b) Srikrishna, A.; Viswajanani, R.; Reddy, T. J.; Vijaykumar, D.; Kumar, P. P. *J. Org. Chem.* **1997**, *62*, 5232. (c) Liaw, D.-J.; Huang, C.-C.; Ju, J.-Y. *J. Polym. Sci., Part A: Polym. Chem.* **2006**, *44*, 3382.
(12) Boivin, J.; da Silva, E.; Ourisson, G.; Zard, S. *Tetrahedron Lett.* **1990**, *31*, 2501.
(13) Takasu, K.; Mizutani, S.; Nogushi, M.; Makita, K.; Ihara, M. *Org. Lett.* **1999**, *1*, 391.
(14) Fraser, R. R.; Swingle, R. B. *Can. J. Chem.* **1970**, *48*, 2065.
(15) Marco-Contelles, J.; Gómez-Sánchez, E.; Samadi, A.; Soriano, E.; Valderas, C.; Álvarez-Pérez, M.; Carreiras, M. C. *Arkivoc* **2010**, (iii), 56–73.
(16) Armstrong, A.; Bhonoah, Y.; Shanahan, S. E. *J. Org. Chem.* **2007**, *72*, 8019.

SCHEME 3

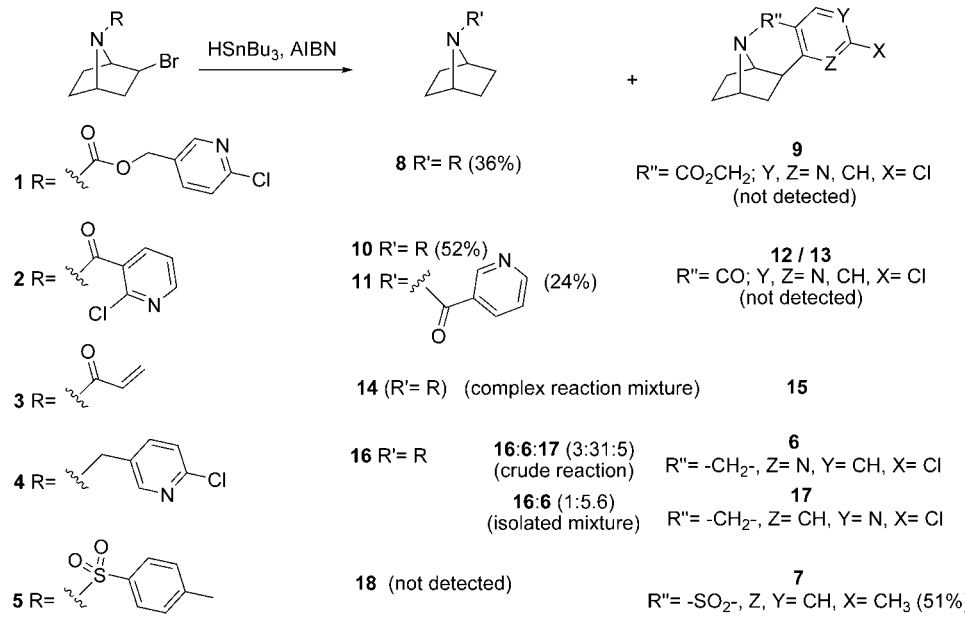

SCHEME 4

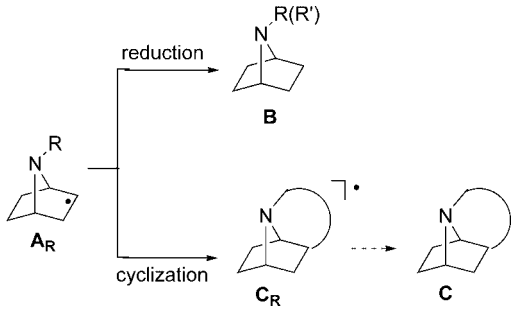

= 1.850 Å) is moderate (17.98 kcal mol^{-1}, Figure 3). In contrast, the intramolecular cyclization is a less favored process from both the kinetic and thermodynamic points of view (Figure 3). The cyclization involves a geometric distortion that is evident from the enhancement of the pyramidalization of the carbamate N ($\Delta \approx +5°$), the closure of the C−O−C−C dihedral angle (from 141.1° to 61.0° and to 54.8° from $\mathbf{1_R}$ to $\mathbf{TS_1}$ and to $\mathbf{9_R}$) and the C−O−C bond angle (from 116.2° to 111.8° and 111.4°, respectively). While the evaluation of the energy penalty accompanying each deformation term is beyond the scope of our analysis, it is obvious that they deeply contribute to raising the energy barrier to the transition state and also to destabilizing the cyclized intermediate (endothermic step by 11.22 kcal mol^{-1}, Table 1).

Although experimental evidence did not indicate other plausible transformations, a competitive pathway can be envisaged from precursor **1**. Thus a 1,6-hydrogen transfer would generate a highly stabilized radical species $\mathbf{1'_R}$ through the transition structure $\mathbf{TS_{1'}}$ (Figure 4). This intramolecular step, however, shows an activation barrier 4.27 kcal mol^{-1} higher

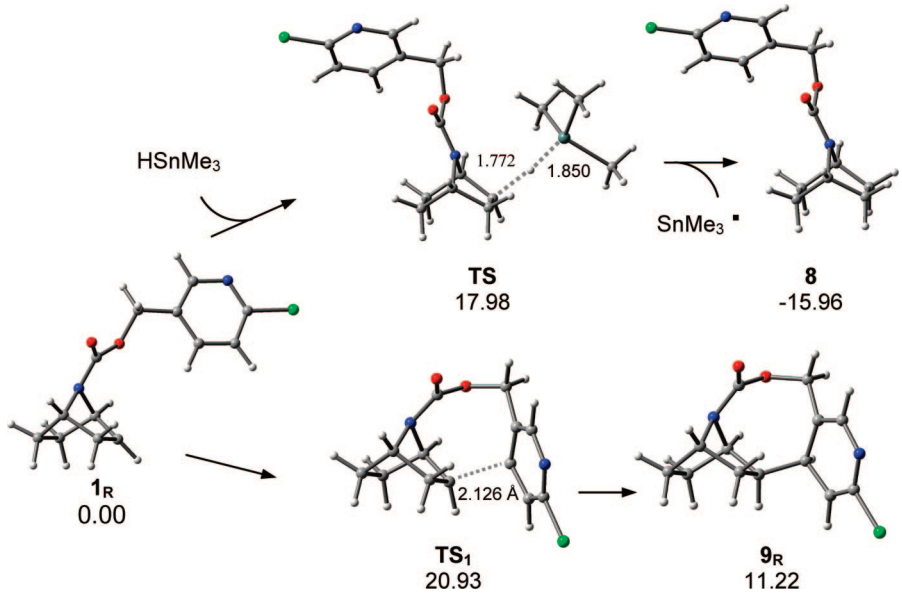

FIGURE 3. Optimized structures for the formation of the reduced species **8** (top) and intramolecular cyclization (bottom) of the reactive radical $\mathbf{1_R}$. Free-energy differences are given in kcal mol^{-1}.

TABLE 1. Thermodynamic Data (in kcal mol^{-1}) in Gas Phase and in Solution for the Formation of Reduced and Cyclized Adducts from the Reactive Radicals Generated from 1−3

precursor	product	$\Delta H^{\ddagger}_{gas}$	ΔH_{gas}	$\Delta G^{\ddagger}_{gas}$	ΔG_{gas}	$\Delta G^{\ddagger}_{sol}$	ΔG_{sol}
$\mathbf{1}_R$	reduced product (**8**)	6.08	−17.21	16.84	−14.39	17.98	−15.96
	cyclization ($\mathbf{9}_R$)	20.06	10.32	22.27	12.61	20.93	11.22
$\mathbf{2}_R$	reduced product (**10**)	4.38	−18.83	16.51	−15.17	17.57	−16.10
	cyclization ($\mathbf{12}_R$)	22.32	7.30	24.87	10.12	22.36	6.86
	cyclization ($\mathbf{13}_R$)	27.86	−2.61	30.62	−0.01	28.63	−2.55
$\mathbf{3}_R$	reduced product (**14**)	5.12	−17.56	15.97	−14.02	17.26	−15.53
	cyclization ($\mathbf{15}_R$)	24.76	−13.78	27.27	−10.96	26.10	−11.76

than that of the intermolecular process (reduction), because of the structural distortion still needed to reach the transition state.

An opposite picture is found for precursor **3** (Figure 5). The pertinent radical intermediate $\mathbf{3}_R$ presents a pendant group considerably shorter than $\mathbf{1}_R$, which implies a stronger pyramidalization of the amide N and opening of the N−C−C bond angle to reach the transition state (from 29.4° to 42.3°; from 116.0° to 119.6° from $\mathbf{3}_R$ to $\mathbf{TS}_3$, respectively). Also, a steric repulsion between the olefinic H and H(C1) has been detected in the transition structure, which cannot be minimized given the chain length. These effects can account for the high energy barrier computed for the cyclization to $\mathbf{15}_R$ (26.10 kcal mol^{-1}), considerably higher than that for the formation of the reduced species **14** (17.26 kcal mol^{-1}, Table 1).

Precursor **2** shows an intermediate linker length, though showing low flexibility, so it should be a more suitable precursor for a successful cyclization. Two kinds of cyclized adducts can be envisaged from the reactive radical $\mathbf{2}_R$ ($\mathbf{12}_R$ and $\mathbf{13}_R$), whose formation implies aromatic positions bearing different substituents (Figure 6). They may proceed through four possible transition structures differing on the approach mode of the aromatic ring (see Supporting Information). The structural distortion found for these structures arises from the N pyramidalization from the reactant intermediate $\mathbf{2}_R$ ($\Delta \approx 8°$) and out-of-plane bending of the H or Cl heteroatom at the bond-forming position, which is higher for the formation of $\mathbf{13}_R$ in order to reduce steric repulsions between the halide atom and the proton at C1 or, alternatively, C3 (40° for the formation of $\mathbf{12}_R$ and 60° for the formation of $\mathbf{13}_R$). As a result, the formation of $\mathbf{12}_R$ is kinetically favored over the formation of $\mathbf{13}_R$ (Table 1).

Nevertheless, the clearly most favorable process is the formation of the reduced species **10**. The activation barrier to reach the transition structure (Sn−H = 1.825, C−H = 1.772 Å) is 17.57 kcal mol^{-1}, about 5 kcal mol^{-1} lower than the preferred cyclization route. These results are in good agreement with the experimental evidence (Scheme 3) and support the key role of steric effects in the cyclization event. Thus, not only is the linker length a critical factor but also its inherent flexibility to allow the interaction with the radical center in the transition state.

Experimental observations revealed that amine **4** afforded a complex reaction mixture (Scheme 3). In the GC/MS analysis of the reaction crude three compounds were detected (**16**,[17] **6**, **17**) in a 3:31:5 ratio. After chromatography we were only able to isolate and characterize an inseparable mixture of **16** and **6** in a 1:5.6 ratio (GC/MS).[15]

The kinetically favored transition structures for the cyclization of radical $\mathbf{4}_R$, driving to the cyclized radicals $\mathbf{6}_R$ and $\mathbf{17}_R$ (see Supporting Information), involve a *staggered* conformation of the methylene tether (Figure 7). Since the halide atom is placed

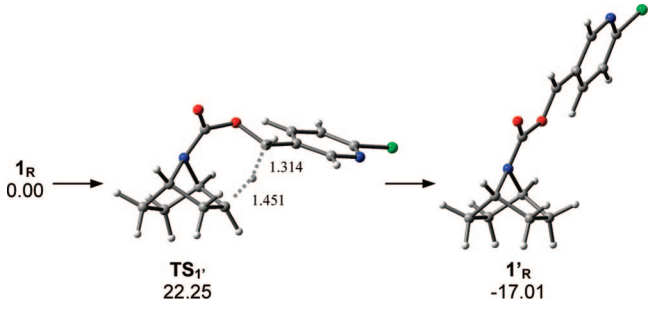

FIGURE 4. Optimized structures for the 1,6-hydrogen migration step to form the radical $\mathbf{1'}_R$. Free-energy differences relative to $\mathbf{1}_R$ are given in kcal mol^{-1}.

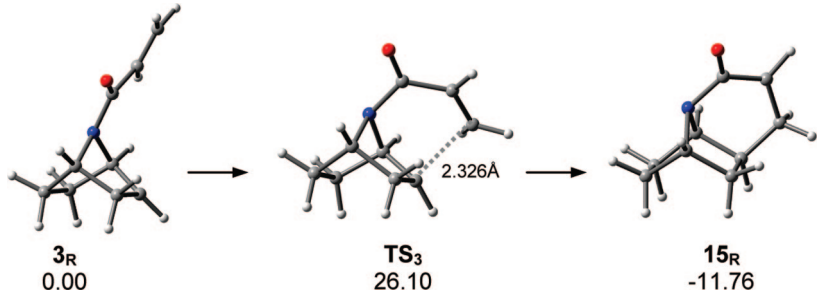

FIGURE 5. Optimized structures for the intramolecular cyclization of the reactive radical $\mathbf{3}_R$.

TABLE 2. Thermodynamic Data (in kcal mol^{-1}) in Gas Phase and in Solution for the Formation of Reduced and Cyclized Adducts from the Reactive Radicals Generated for 4 and 5

precursor	product	$\Delta H^{\ddagger}_{gas}$	ΔH_{gas}	$\Delta G^{\ddagger}_{gas}$	ΔG_{gas}	$\Delta G^{\ddagger}_{sol}$	ΔG_{sol}
$\mathbf{4}_R$	Reduced product (**16**)	7.39	−18.02	18.42	−13.98	21.00	−14.45
	Cyclization ($\mathbf{6}_R$)	12.79	−4.88	15.62	−2.11	13.53	−4.36
	Cyclization ($\mathbf{17}_R$)	13.62	−0.80	16.52	2.05	14.00	−0.72
$\mathbf{5}_R$	Reduced product (**18**)	6.43	−17.02	17.69	−13.93	18.70	−13.31
	Cyclization ($\mathbf{7}_R$)	11.09	−5.17	13.23	−2.67	7.23	−8.11

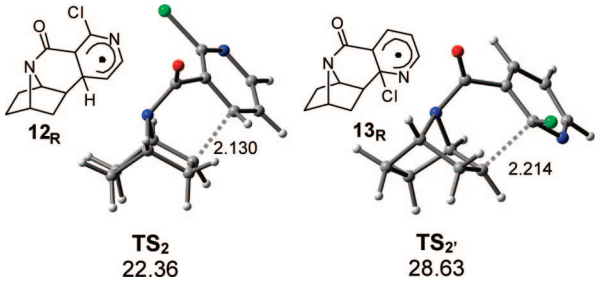

FIGURE 6. Optimized transition structures $\mathbf{TS_2}$ and $\mathbf{TS_{2'}}$ for the intramolecular cyclization to $\mathbf{12_R}$ and $\mathbf{13_R}$, respectively, of the reactive radical $\mathbf{2_R}$.

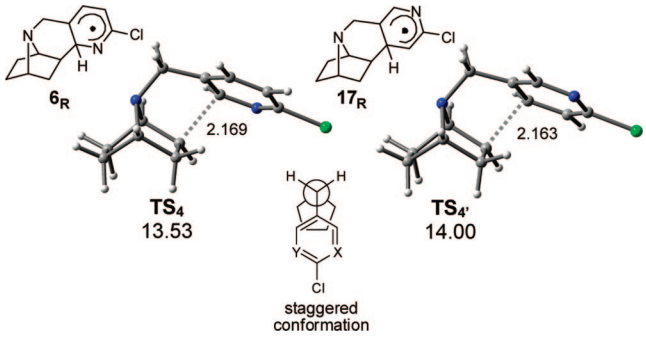

FIGURE 7. Optimized transition structures $\mathbf{TS_4}$ and $\mathbf{TS_{4'}}$ for the intramolecular cyclization to $\mathbf{6_R}$ and $\mathbf{17_R}$, respectively, of the reactive radical $\mathbf{4_R}$.

at the *para* position in both intermediates, it is expected that both routes involve similar barriers. Given that the installed functional group is an amine, the nitrogen is intrinsically pyramidalized, and therefore no further pyramidalization is needed to achieve the transition state ($\Delta < +1.0°$). Analogously, the bond angle N−C−C is kept along the reaction coordinate, and only a marginal closing has been detected in the transition structure and in the cyclized adduct ($\Delta < -0.5°$). This low conformational distortion accounts for the reduced activation barriers computed in comparison with that for amide precursor (about 9 kcal mol^{-1} lower for the most favorable transition structure, $\mathbf{TS_4}$). Accordingly, the cyclization is slightly exothermic as a result of this low structural distortion.

Remarkably, the cyclization to $\mathbf{6_R}$ is slightly more favorable than to its isomer $\mathbf{17_R}$ from the kinetic and thermodynamic viewpoint (Table 2), although the small energy differences would suggest the formation of both radical species.

On other hand, the formation of the reduced species **16** by H-abstraction proceeds, as shown above, through a slightly asymmetrical transition structure (Sn−H =1.815, C−H = 1.786 Å). Unexpectedly, this step takes place with an activation barrier of 21.00 kcal mol^{-1}, 3.5 kcal mol^{-1} higher than that for **10** without apparent structural or electronic reasons, so we have come to suspect that a conformational effect is at play in this step. Thus, a high-energy conformer has likely been selected in the broad conformational space. In any case, a comparison between amide **2** and amine **4** strongly suggests that the intramolecular cyclization route for the latter emerges as not only a possible but also a favored process, in good agreement with the experimental findings.

(17) Cheng, J.; Zhang, C.; Stevens, E. D.; Izenwasser, S.; Wade, D.; Chen, S.; Paul, D.; Trudell, M. L. *J. Med. Chem.* **2002**, *45*, 3041.

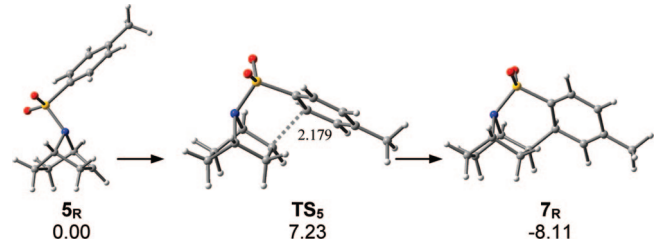

FIGURE 8. Optimized structures for the cyclization of the radical $\mathbf{5_R}$. Free-energy differences are given in kcal mol^{-1}.

Concerning the intramolecular free radical cyclization of sulfonamides,[18] the tributyltin hydride mediated cyclization of $\mathbf{5_R}$ provided the ring-closure derivative **7** in 51% yield.[15] This is not an unexpected result since the computed length of N−S (1.695 Å) and S−C (1.793 Å) single bonds allows an easy access to the transition state, with a minor geometric distortion (N pyramidalization, +1.5°; closing of the N−S−C bond angle, −3.5°, on going from $\mathbf{5_R}$ to $\mathbf{TS_5}$, Figure 8) and reduces the annular tension of the forming cycle. Accordingly, the cyclization onto the tosyl group to afford the radical intermediate $\mathbf{7_R}$, which is an exothermic process (−8.11 kcal mol^{-1}), shows a low activation barrier, 7.23 kcal mol^{-1} (Table 2). The formation of the reduced species **18** takes place with an activation barrier 11.5 kcal mol^{-1} higher (18.70 kcal mol^{-1}) than the intramolecular cyclization to **7**. Therefore, the presence of a sulfonyl group widens the energy gap between the H-abstraction and cyclization transition structures which draws the former as a hardly competitive process.

On other hand, an *ipso* radical substitution from precursors $\mathbf{5_R}$ appears as a possible reaction under free-radical conditions (Figure 9).

Calculations have revealed that the trapping of the *ipso* carbon by the radical center (Figure 9) is kinetically viable since it involves a relatively low activation barrier of 11.75 kcal mol^{-1}. However, this value is 4.5 kcal mol^{-1} higher than that computed for the less strained cyclization over the neighboring carbon ($\mathbf{TS_5}$). The formation of $\mathbf{19_R}$ is endothermic (by 5.01 kcal mol^{-1}) mostly due to the annular tensión on the spirocyclic adduct, as suggested by the N pyramidalization (+7.0°), lengthening of the S−C bond (+0.063 Å), and the closing of the bond angle N−S−C (−2.1°) from $\mathbf{5_R}$. This intermediate may evolve to the *ipso* substituted adduct ($\mathbf{20_R}$) (Figure 9) or to the known tricycle $\mathbf{7_R}$. The formation of $\mathbf{20_R}$ appears as a barrierless process from $\mathbf{19_R}$, probably because of the tension released. In any case, the preferential formation of $\mathbf{7_R}$ takes place through the lowest energy transition structure $\mathbf{TS_5}$.

In summary, although this process to $\mathbf{20_R}$ is kinetically viable under the reaction conditions, it would be disfavored over the formation of the cyclized product $\mathbf{7_R}$, in agreement with the experimental observations.

At this point, we wondered whether these favorable results for the cyclization process of **5** are due only to the selected linker or if the type of aromatic ring has also an influence. Hence, we have decided to compare **5** with the pyridinic model **21** in order to assess the ring effect. The data point out a favored intramolecular cyclization for **5**: cyclization barrier of 7.23 kcal mol^{-1} to afford $\mathbf{7_R}$ versus 12.54 and 14.93 kcal mol^{-1} to $\mathbf{22_R}$

(18) (a) Motherwell, W. B.; Pennell, A. M. K. *J. Chem. Soc., Chem. Commun.* **1991**, 877. (b) da Mata, M. L. E. N.; Motherwell, W. B.; Ujjainwalla, F. *Tetrahedron Lett.* **1997**, *38*, 137. (c) da Mata, M. L. E. N.; Motherwell, W. B.; Ujjainwalla, F. *Tetrahedron Lett.* **1997**, *38*, 141.

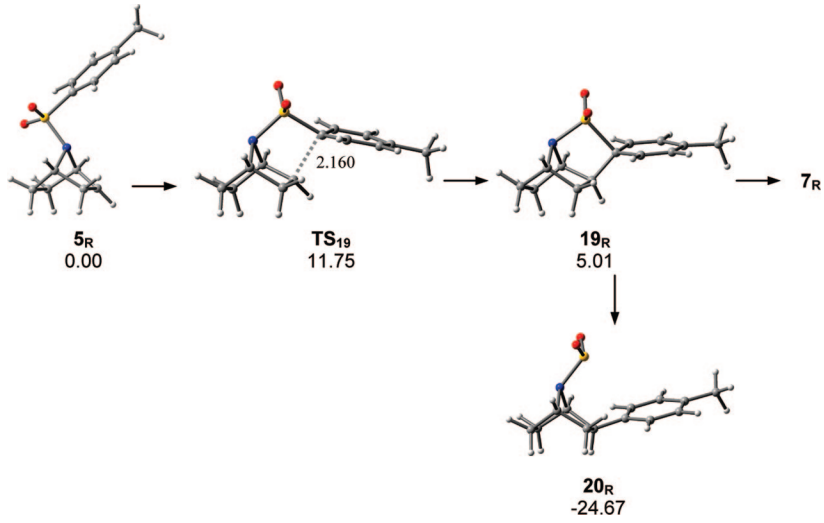

FIGURE 9. Optimized structures for the *ipso* radical substitution from $\mathbf{24_R}$. Free-energy differences relative to $\mathbf{20_R}$ are given in kcal mol^{-1}.

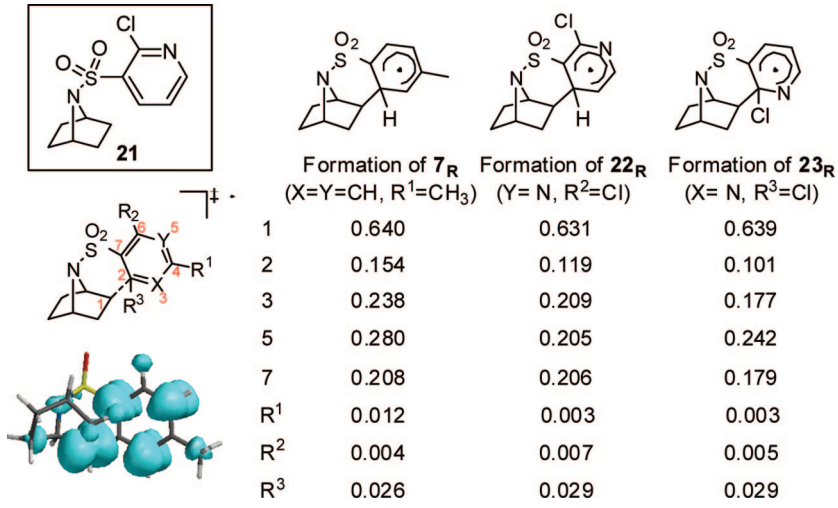

	Formation of $\mathbf{7_R}$ (X=Y=CH, R^1=CH_3)	Formation of $\mathbf{22_R}$ (Y= N, R^2=Cl)	Formation of $\mathbf{23_R}$ (X= N, R^3=Cl)
1	0.640	0.631	0.639
2	0.154	0.119	0.101
3	0.238	0.209	0.177
5	0.280	0.205	0.242
7	0.208	0.206	0.179
R^1	0.012	0.003	0.003
R^2	0.004	0.007	0.005
R^3	0.026	0.029	0.029

FIGURE 10. Spin density on the transition structures leading to radicals $\mathbf{7_R}$, $\mathbf{22_R}$, and $\mathbf{23_R}$.

and $\mathbf{23_R}$ (Figure 10), respectively. The computed spin density on the pertinent transition structures reveals the expected spin delocation on the *ortho* and *para* sites (regarding the forming bond position), although it is more efficient for the carbo- than for the heteroaromatic ring, which may account, at least in part, for the high stability of the transition structure $\mathbf{TS_5}$.

Conclusions

We have studied by DFT methods the mechanisms of intramolecular free radical reactions for the synthesis of conformationally constrained epibatidine analogues.[15] Computational analyses have been carried out to explain the mechanism of this reaction and the key effect of the 7-nitrogen protecting group as tethering chain on the outcome of these cyclizations. The calculations suggest that this linker to the aromatic entity not only must be long enough to be trapped by the radical center but also possess a high flexibility. This justifies that carbamates or amides inhibit the process and yield major reduced, uncyclized, reaction products, as the limited chain flexibility gives rise to a high activation barriers. Unlike these groups, the *N*-sulfonyl and the *N*-arylmethyl functional motifs, inherently flexible, involve a lower activation barrier for the cyclization than for the reduction, which is supported by the fact that they afforded major cyclized products.[15] Therefore, theoretical calculations should be a valuable tool to select proper precursors for future synthesis of new epibatidine analogues.

Experimental Section

Computational Methods. All calculations were carried out with Gaussian98 and Gaussian03 packages.[19] All minima and transition states involved were fully optimized with the B3LYP hybrid functional. [20] The standard 6-31G(d) basis set has been applied for all the atoms except Sn, which has been described by the LANL2DZ basis set,[21] where the innermost electrons are replaced by a relativistic ECP. To get reliable energy values, single-point energy calculations have been carried out with the extended 6-311G(2d,p) basis set on the optimized structures. Zero-point energies (ZPEs) and thermal contributions to thermodynamic functions and activation parameters, as well as harmonic frequencies, were computed at the same level of theory on the optimized

(19) (a) *Gaussian 98*, Revision A.11; Frisch M. J. et al.; Gaussian, Inc.: Pittsburgh, PA, 2001. (b) *Gaussian 03*, Revision B.03; Frisch, M. J., et al.; Gaussian, Inc.: Wallingford, CT, 2003 (see Supporting Information for complete references).

(20) (a) Lee, C.; Yang, W.; Parr, R. *Phys. Rev. B* **1988**, *37*, 785–789. (b) Becke, A. *J. Chem. Phys.* **1993**, *98*, 5648.

(21) Hay, P. J.; Wadt, W. R. *J. Chem. Phys.* **1985**, *82*, 270.

structures. Intrinsic reaction coordinate (IRC) calculations[22] at the optimization level of theory were carried out on the transition states to obtain the two minima on the potential energy surface (PES) connected by each transition state. A comparison with other theoretical models and basis sets has concluded that this combination provides reliable results at a reasonable computational cost (see Supporting Information for details).

Solvent effects have been taken into account by the self-consistent reaction field (SCRF) method using the so-called conductor polarizable continuum model (CPCM)[23] as implemented in Gaussian03, in which the solvent is represented by an infinite dielectric medium characterized by the relative dielectric constant of the bulk. A relative permittivity of 2.379 was assumed to simulate toluene as solvent. Natural bond orbital (NBO) analyses[24] have been performed by the module NBO v.3.1 implemented in Gaussian03 to evaluate the NPA charges and hyperconjugation effects on the optimized structures.

Acknowledgment. J.M.-C. thanks MEC (Spain) for a grant (SAF2006-08764-C02-01), Comunidad de Madrid (S/SAL-0275-2006), Instituto de Salud Carlos III [RED RENEVAS (RD06/0026/1002)], and CSIC (2008CR0004). The authors thank E. Gómez for helpful discussions and the Centro de Supercomputación de Galicia (CESGA) for generous allocation of computing resources.

Supporting Information Available: Comparison with other theoretical model and basis sets, additional results on the radical reactions, Cartesian coordinates of the optimized structures and full ref 19. This material is available free of charge via the Internet at http://pubs.acs.org.

JO900225F

(22) (a) Fukui, K. *Acc. Chem. Res.* **1981**, *14*, 363. (b) González, C.; Schlegel, H. B. *J. Phys. Chem.* **1990**, *94*, 5523.

(23) (a) Barone, V.; Cossi, M. *J. Phys. Chem. A* **1998**, *102*, 1995–2001. (b) Cossi, M.; Rega, N.; Scalmani, G.; Barone, V. *J. Comput. Chem.* **2003**, *24*, 669.

(24) *NBO Version 3.1*; Glendening, E. D., Reed, A. E., Carpenter, J. E., Weinhold, F. For original literature, see:(a) Reed, A. E.; Weinhold, F. *J. Chem. Phys.* **1983**, *78*, 4066. (b) Reed, A. E.; Curtiss, L. A.; Weinhold, F. *Chem. Rev.* **1988**, *88*, 899.